Knight, M., Damion, R., McGarry, B., Bosnell, R., Jokivarsi, K. T., Grohn, O. H. J., Jezzard, P., Harston, G. W. J., Carone, D., Kennedy, J., El-Tawil, S., Elliot, J., Muir, K. W., Clatworthy, P., & Kauppinen, R. (2019). Determining T2 relaxation time and stroke onset relationship in ischaemic stroke within apparent diffusion coefficient-defined lesions. A user-independent method for quantifying the impact of stroke in the human brain. *Biomedical Spectroscopy and Imaging*, *8*(1-2), 1-18. https://doi.org/10.3233/BSI-190185

Peer reviewed version

License (if available):
Unspecified

Link to published version (if available):
10.3233/BSI-190185

Determining T2 relaxation time and stroke onset relationship in ischaemic stroke within apparent diffusion coefficient-defined lesions. A user-independent method for quantifying the impact of stroke in the human brain

Michael J. Knight[1], Robin A. Damion[1], Bryony L. McGarry[1], Rose Bosnell[2], Kimmo T. Jokivarsi[3], Olli H.J. Gröhn[3], Peter Jezzard[4], George W.J. Harston[5], Davide Carone[5], James Kennedy[5], Salwa El-Tawil[6], Jennifer Elliot[6], Keith W. Muir[6], Philip Clatworthy[2] and Risto A. Kauppinen[1]

[1]School of Experimental Psychology, University of Bristol, Bristol, UK; Stroke Medicine, Southmead Hospital, North Bristol NHS Trust, Bristol, UK; [2]Stroke Neurology, Southmead Hospital, North Bristol NHS Trust, Bristol, UK, [3]Department of Neurobiology, A.I. Virtanen Institute, University of Eastern Finland, Kuopio, Finland, [4]Oxford Centre for Functional MRI of the Brain, Nuffield Department of Clinical Sciences, University of Oxford, Oxford UK, [5]Acute Stroke programme, Radcliff Department of Medicine, University of Oxford, UK, [6]Institute of Neuroscience and Psychology, Queen Elizabeth University Hospital, University of Glasgow, Scotland

Address for correspondence: Professor Risto Kauppinen
School of Experimental Psychology
University of Bristol
12a Priory Rd
Bristol BS8 1TU
UK
psrak@bristol.ac.uk
tel: +44 117 928 8461

BACKGROUND AND OBJECTIVE:

In hyperacute ischaemic stroke, T2 of cerebral water increases with time. Quantifying this change may be informative of the extent of tissue damage and onset time. Our objective was to develop a user-unbiased method to measure the effect of cerebral ischaemia on T2 to study stroke onset time-dependency in human acute stroke lesions.

METHODS:

Six rats were subjected to permanent middle cerebral occlusion to induce focal ischaemia, and a consecutive cohort of acute stroke patients (n = 38) were recruited within 9 hours from symptom onset. T1-weighted structural, T2 relaxometry, and diffusion MRI for apparent diffusion coefficient (ADC) were acquired. Ischaemic lesions were defined as regions of lowered ADC. The median T2 difference (ΔT2) between lesion and contralateral non-ischaemic control region was determined by the newly-developed spherical reference method, and data compared to that obtained by the mirror reference method. Linear regressions and receiver operating characteristics (ROC) were compared between the two methods.

RESULTS:

ΔT2 increases linearly in rat brain ischaemia by 1.9 ± 0.8 ms/h during the first 6 hours, as determined by the spherical reference method. In patients, ΔT2 linearly increases by 1.6 ± 1.4 and 1.9 ± 0.9 ms/h in the lesion, as determined by the mirror reference and spherical reference method, respectively. ROC analyses produced areas under the curve of 0.83 and 0.71 for the spherical and mirror reference methods, respectively.

CONCLUSIONS:

Data from the spherical reference method showed that the median T2 increase in the ischaemic lesion is correlated with stroke onset time in a rat as well as in a human patient cohort, opening the possibility of using the approach as a timing tool in clinics.

Keywords: T2 relaxation time, diffusion MRI, stroke onset time, acute ischaemic stroke

Running head: Stroke onset time dependent T2 relaxation time change in ADC lesion

1. Introduction

The mainstay of hyperacute ischaemic stroke treatment is reperfusion therapy, including intravenous thrombolysis and mechanical intra-arterial thrombectomy. Both treatments are effective at reducing disability but only if initiated sufficiently soon after the onset of ischaemia [20]. As time elapses the likelihood of benefit from treatment declines and the risk of haemorrhagic complications of treatment increases. At present thrombolysis using recombinant tissue plasminogen activator (rtPA) is licensed up to 4.5 hours after onset of symptoms and is therefore rarely used when the time of symptom onset is unknown such as when symptoms become apparent on waking (often termed “wake-up stroke”). Mechanical thrombectomy using stent-retrievers is a more recent and highly effective treatment for ischaemic stroke caused by occlusion of a major intra-cerebral vessel. Again, the benefit of treatment declines with duration of ischaemia; some current guidelines recommend that treatment should commence within 6 hours of symptom onset.

A recently evaluated approach using MRI compares hyperintense signal on diffusion weighted imaging (DWI) with T2 FLAIR [24]: a bright DWI signal that is not apparent on FLAIR has reasonable specificity for onset within the preceding 4.5 hours, and visual assessment of this “DWI-FLAIR mismatch” formed the basis for patient selection in the WAKE-UP clinical trial, which demonstrated significant improvement in outcome when such patients were treated with intravenous rtPA [26]. The subjective nature of MRI interpretation using this approach may, however, limit uptake. An alternative is to make use of quantitative T2 mapping, which seeks to parameterise the T2 in an image of its values [27]. The change in T2 underpins the FLAIR signal intensity changes. Animal models using rats [7, 16], cats and primates, as well as theoretical models [13] have demonstrated that the T2 relaxation time increases in ischaemic tissue roughly linearly at ~1 – 2 ms/hour (after an initial drop) for the first few hours after onset consistently across species [9]. There is evidence for a similar rate of increase in humans [21]. However, measurement of the change of T2 from a baseline (unmeasured, pre-ischaemic) state becomes very difficult in the brains of higher species, for there is considerable anatomical variation in T2, which varies by more than the change caused by ischaemia. For example, the average T2 in the corticospinal tracts is about 10 – 15 ms higher than in other white matter structures [12], a larger difference than the anticipated T2 change during the first 6 hours of ischaemia.

The purpose of this study is to demonstrate the viability of a new user-independent method of estimating images of the pre-ischaemic brain based on images of the ischaemic brain, and therefore preparing images of the change caused by ischaemia. The approach prepares

images of the change in any “imageable” quantity. We demonstrate that, in particular, images of the pre-ischaemic ADC and T2 relaxation time may be calculated and thereby the change caused by ischaemia to be determined. We validate our method in a rat model of cerebral ischaemia and apply it in a cohort of human acute ischaemic stroke patients. We obtain estimates of the probable T2 and ADC change with time across the entire ADC-demarcated lesions, revealing heterogeneity of T2 change. We propose that the median T2 change is a good reporter of lesion age, for it correlates well with stroke onset time.

2. Methods

2.1. Animal data acquisition and processing

Male Wistar rats (n=6, weight 200 – 300 g) were exposed to permanent middle cerebral artery occlusion (MCAo) [15] and scanned by a procedure described in [16]. The occluding thread was left in place for the duration of the MRI scanning and the animal was sacrificed thereafter by decapitation in deep isoflurane anaesthesia. Animal procedures were conducted according to European Community Council Directives 86/609/EEC guidelines and approved by the Animal Care and Use Committee of the University of Eastern Finland.

A horizontal 9.4 T Agilent MRI scanner (Agilent, Palo Alto, CA, US) equipped with an actively decoupled linear volume transmitter and quadrature receiver coil pair (RAPID Biomedical GmbH, Rimpar, Germany) was used. Each measurement comprised a 3-plane diffusion-weighted sequence (b-values = 0, 400, 1040 s/mm^2; TE = 36 ms, TR = 2000 ms) and a multi-echo spin-echo sequence (12 echoes 10 ms inter-echo spacing, TR = 2000 ms). Twelve slices were imaged with the following parameters: 0.5 mm gap, slice thickness = 1 mm, FOV = 2.56 cm x 2.56 cm was covered by 128 x 256 points. Measurements, each taking ~20 minutes, were made at times commencing 60, 120, 180 and 240 minutes after MCAo.

2.2. Human data acquisition and processing

The study received ethical approval to accrue acute stroke patients from South West Frenchay Research Ethics Committee for participants in Bristol (reference 13/SW/0256), Scotland A REC for participants in Glasgow (reference 16/SS/0223), and UK National Research Ethics Service Committee for participants in Oxford (references 12/SC/0292 and 13/SC/0362). Informed consent was received either from participants or their legal representative prior to enrolment to the study. Stroke patients were recruited if they presented in the emergency department with witnessed symptom onset so that MRI scans could be completed with 9 hours of onset. Details of the human acute stroke cohort is given in Table 1. The project was carried out in accordance with the Declaration of Helsinki.

All MRI scans on stroke patients were acquired using 3T scanners: Philips Achieva (Bristol); Siemens Magnetom Prisma (Glasgow); Siemens Magnetom Verio (Oxford). At each of the three sites, a 32-channel head-coil was used. The details of the T1, diffusion, and T2 pulse sequences and acquisition parameters are given in Table 2.

Quantitative T2 maps were obtained by fitting a mono-exponential decay on a voxel-wise basis. All echoes of the TE series were summed to produce a sum-over-echoes image, which was subject to bias field correction [29] using FSL FAST (FMRIB, Oxford, UK).

For diffusion-weighted data with a single b-value, apparent diffusion coefficient (ADC) maps were calculated using

$$ADC = -\ln\left(S/S_0\right)/b$$

where *S* and S_0 are the signal intensities with and without diffusion weighting respectively and *b* is the b-value. For data using three orthogonal diffusion-sensitising gradients at a common b-value, ADC maps were obtained from

$$ADC = -\ln(S_1 S_2 S_3 / S_0^3)/3b$$

where $S_{1,2,3}$ are the signal intensities at the 3 orthogonal directions, S_0 as before, b as before.

Diffusion-weighted data (Glasgow) with twenty independent diffusion-gradient directions (b=1000 mm^2/s) and three b=0 images were processed using FSL DTIFIT from which the mean-diffusivity maps provided the ADC values.

2.3 Lesion identification and mask creation

Brain-extracted images were analysed following rigid-body co-registration to the MNI frame at 1 mm isotropic resolution resampling using FSL FLIRT [6]. The ADC maps were first co-registered to T2-weighted space by a non-linear registration of the S_0 image to the sum-over-echoes image using FSL FNIRT. In this co-registered space, the ADC lesion was demarcated as follows.

A reference tissue mask was first created by the application of thresholds on T2 and *ADC* to reduce the contribution from CSF. These thresholds were typically 30 ms < T2 < 200 ms, 0.1 $\mu m^2\ ms^{-1}$ < *ADC* < 1.5 $\mu m^2\ ms^{-1}$. A lesion tissue mask was then created in two stages. First, the thresholds (which could vary in individual cases) 30 ms < T2 < 200 ms, 0.2 – 0.4 $\mu m^2\ ms^{-1}$ < *ADC* < 0.55 – 0.60 $\mu m^2\ ms^{-1}$ were applied and, secondly, the additional criterion—that the *ADC* should be less than one half-width half-maximum from the median *ADC* of the reference tissue—was applied. The lesion mask was then further refined by removing all but the largest contiguous cluster (or clusters, in the cases of more than one lesion). This lesion mask was then removed from the reference tissue mask to create a non-lesion tissue mask.

2.4 Algorithm for T2 change due to ischaemia

To calculate the change in T2 due to ischaemia for each voxel in the lesion, it is necessary to provide reference, T_2^{R}, values to which each voxel's ischaemic T2 can be compared. That is, an estimate is needed for the *pre*-ischaemic T2 within each voxel of the lesion. Reference T2 values have previously been obtained [7, 21] from single contralateral voxels in the unaffected hemisphere. However, such a method is prone to error due to the imperfect symmetry and heterogeneity of the human brain. To circumvent this issue, pre-ischaemic (reference) T2 values are calculated from voxels within reference spheres of a given radius, centred on the contralateral voxel.

To achieve this, the algorithm adopts the premise that, in the hyperacute phase of ischaemia, the T2-*weighted* images are relatively insensitive to ischaemia and therefore the intensity values within each voxel of the lesion are sufficiently close to their pre-ischaemic values to be taken as estimates for their pre-ischaemic values. With this premise, the intensity I^{L} of a lesion voxel can be used to condition the reference T2 for that voxel.

Despite the relative insensitivity to ischaemia of the T2-weighted intensities, there may still be a dependency between the intensities and T2 values in normal brain tissue within any given region. Therefore, it is possible to obtain an estimate of pre-ischaemic T2 by using the intensity estimate of the pre-ischaemic intensity (i.e., the ischaemic intensity value I^{L}) to calculate a type of conditional expectation of T2 values within the reference sphere of a given lesion voxel. That is, an estimate of the pre-ischaemic T2 is obtained by the mean T2 of normal brain tissue within a reference sphere, conditioned by the intensity value I^{L} of the ischaemic lesion voxel.

To effect the conditioning, we employ a penalty function $F(I)$ which weights the sum over the T2 values associated with voxels indexed by k in a reference sphere S. Therefore, let the reference T2 be given by

$$T_2^R = \sum_{k=1}^{N_S} T_{2,k} F(I_k)$$

where N_S is the number of voxels in the reference sphere S, and where the penalty function is normalised by $\sum_{k=1}^{N_S} F(I_k) = 1$. This may be equivalently expressed as

$$T_2^{\mathrm{R}} = \frac{\langle T_2 F(I) \rangle}{\langle F(I) \rangle} = \frac{\int \mathrm{d}I \; F(I) P(I) \int \mathrm{d}T_2 \; T_2 P(T_2|I)}{\int \mathrm{d}I \; F(I) P(I)} = \frac{\int \mathrm{d}I \; F(I) P(I) \langle T_2|I \rangle}{\int \mathrm{d}I \; F(I) P(I)}$$

where the integrals are over the values contained in the reference sphere S, $P(I)$ is the probability density for the intensities, $P(T_2|I)$ is the conditional probability density for T2 given the intensity I, and $\langle T_2|I\rangle$ is the mean T2 conditioned on I.

In the limit that $F(I)$ is constant, T_2^{R} is the unweighted mean T2 of all the voxels in the reference sphere. Conversely, in the limit that $F(I)$ becomes a delta-function positioned at I^{L}, $T_2^{\mathrm{R}} = \langle T_2|I^L\rangle$. However, in the present context, the use of a delta-function is impractical. Instead, a penalty function of finite width is employed, such that

$$F(I_k) = A^L \exp\left(-\left[\frac{I_k - I^L}{I^L}\right]^2 / 2\sigma^2\right)$$

where A^{L} is a normalisation constant which depends on each reference sphere associated with each lesion voxel. With this penalty function, T_2^{R} can be regarded as the mean T2 within the reference sphere, conditioned on a Gaussian neighbourhood of I^{L}.

With this method of obtaining the reference, T_2^{R}, for a given reference sphere associated with a lesion voxel and its T2-value, T_2^{L}, the estimated change is simply given by $\Delta T_2 = T_2^L - T_2^R$. This method can also be used to estimate changes in other MRI parameters, such as the ADC value.

In our implementation of this algorithm, the T2-weighted intensities were obtained from the sum-over-echoes image after bias-field correction. The reference sphere radius and penalty function width, σ, were obtained by optimisation on each patient data set by using the unaffected tissue in the hemisphere of the lesion to minimise the function $f(\beta) = \mathrm{mad}(\Delta T_2) + \beta|\mathrm{median}(\Delta T_2)|$, with $\beta = 5$, where ΔT_2 is the calculated change in T2, and $\mathrm{mad}(\Delta T_2)$ is the median absolute deviation (MAD). The value of β was chosen so that both summands had approximately equal weight.

2.5. Mirror reference approach

We used a method modified from that proposed by Siemonsen et al. [21] to determine a reference volume from the contralateral non-ischaemic hemisphere, but without the need for manual adjustments. Since all image processing was performed in the MNI frame, the midline of the brain is consistently defined. Therefore, the lesion mask (see section above) can simply be reflected about the midline and then logically combined with the non-lesion tissue mask to ensure that this contralateral (mirror reference) mask also contains only white and grey matter

tissue. T2 statistics could then be easily compared between the lesion and the contralateral mask regions.

2.6. Statistical Analysis

All linear regressions were unweighted and performed within MATLAB (Release 2016b, The MathWorks, Inc., Natick, MA, US) using *fit* to obtain the fitting parameters, confidence intervals on the parameters, and the correlation coefficient, r^2. Two-tailed t-tests on the null hypothesis for the gradient were conducted in the usual manner using the correlation coefficient and the degrees of freedom (d_f=33) to produce the quoted p-values. MATLAB's *predint* was used to produce the observational 95% confidence intervals in the regression plots.

Using SigmaPlot Version 13.0 (Systat Software, San Jose, CA, US), Receiver Operating Characteristic (ROC) curves were computed to determine the overall abilities of the spherical and mirror reference methods in distinguishing between patients scanned within ($\leq$) and beyond ($>$) 4.5 hours from symptom onset. Areas under the ROC curves (AUCs) were also calculated and statistically compared using the non-parametric approach for correlated ROCs [4].

3. Results

3.1. Basics for the spherical reference method

In Figure 1 we show examples of the spherical reference method using scans from an ADC-negative patient. It is demonstrated that the spherical reference method is selective (Figure 1c) for voxels which have similar T2-weighted intensity to the voxel of interest.

3.2. *Application to the rat MCAo*

Figure 2 shows example T2 and ADC maps for a rat during MCAo as well as the corresponding ΔT2 and ΔADC maps calculated using the voxel-wise parameter change algorithm. The lesions are visible in the ADC maps (and expand with time), and likewise visible as a negative ΔADC in the ΔADC images. This effectively validates the algorithm. In the corresponding ΔT2 image, the ΔT2 in the vicinity of the lesion is generally positive, and more so at 4 hours than 1 hour. Hemispheric images are shown since the non-lesion hemisphere is used to model the lesion hemisphere.

Figure 3a provides an example of the shifting ΔT2 histogram with time in a MCAo rat, calculated with the voxel-wise algorithm. The right-shift at each time point is evident. It is also clear that there is a distribution of T2 changes across a lesion at any time point, so that not all voxels are equally affected by ischaemia. The width of a ΔT2 histogram, however, is determined not only by the heterogeneity of a lesion, but also by the error in the algorithm's model for the pre-ischaemic state, and by imprecision of measurement of T2. The distributions cannot be less wide than the latter factor. Nonetheless, the width of a ΔT2 distribution provides an *estimate* of the heterogeneity of T2 change caused by ischaemia. This is a critical advantage of the spherical reference method over other T2 MRI approaches.

Figure 3b shows the change in median ΔT2 with time for the 6 rats, using the MAD of their ΔT2 distributions as uncertainties. The rate of increase of median ΔT2 longitudinally is quite similar in the sampled time range. Cross-sectionally, however, there is variation. This variation appears to be determined by un-sampled early-time evolution and introduces considerable uncertainty into any cross-section estimate of onset time. From this sample, there is at least 5 ms median ΔT2 variation four hours after occlusion.

3.3. Application to human acute stroke

Figure 4 shows the result of the spherical reference method applied to calculate ΔADC and ΔT2 images for a human acute ischaemic stroke patient. The lesion is visible as a low-ADC region in the diffusion image and is likewise visible as a negative ΔADC in the ΔADC image, thereby validating the algorithm in humans. In the corresponding ΔT2 image, the ΔT2 in the vicinity of the lesion is generally positive. Examples of ΔT2 distributions for a stroke lesion (Figure 4f) and the surrounding normal brain parenchyma (Figure 4e) are also shown. These demonstrate that the ΔT2 is centred very close to zero in brain regions in which there is no ischaemia or other neurological disease, whereas in the lesion a shift to right is evident.

Figure 5 shows the cross-sectional relationships between reported onset time and parameters derived from the voxel-wise algorithm. Figure 5a demonstrates a positive correlation between stroke onset time and median ΔT2. We also see that the fit is not perfect, with the median ΔT2 deviating from the fit by a cross-sectional variation larger than that seen in rats. The widths of ΔT2 distributions are also wider in humans, the median RMS errors from linear fits being 5.7 ms, and 1.9 ms in rats. This may reflect greater heterogeneity of the lesion (ischaemia affects different voxels even more unequally in humans), the higher field strength used for the rat model, and/or greater uncertainty in the algorithm's model for the pre-ischaemic state. Interestingly, the non-thrombolysed data points appear to fall almost to a flat line vs time of onset (Figure 5a).

The linear model for the relationship between median ΔT2 and onset time in cross-sectional human data (1.9 ± 0.9 ms/h) is remarkably similar to that obtained in the rat cohort (1.92 ± 0.78 ms/h) when analysed as a group (errors quoted are 95% confidence intervals), RMS error 5.8 ms. Figure 5b shows a plot of the difference in median T2 between the lesion and its contralateral mirror region. A linear regression on this data gives a gradient of 1.6 ± 1.4 ms/h with an RMS error of 8.7 ms. Normalised T2-weighted intensity difference shows no time dependency, as the slope of the line against time of onset is not different from zero (Figure 5c).

Of the 38 patients, 25 were thrombolysed prior to MRI (Table 1) as part of standard of care. As rtPA may alter permeability of blood-brain-barrier, ADC was measured both in the stroke lesion and in the contralateral reference region. In the stroke lesions, the median ADC was found to be 0.51 ± 0.41 $\mu m^2\ ms^{-1}$ and 0.55 ± 0.24 $\mu m^2\ ms^{-1}$ for the thrombolysed and non-thrombolysed patients, respectively. In the reference volumes, the corresponding median

ADCs were 0.79 ± 0.41 $\mu m^2 ms^{-1}$ and 0.78 ± 0.60 $\mu m^2 ms^{-1}$. These values suggest that rtPA did not significantly affect the tissue state.

ROC curves for the spherical and mirror reference approaches are displayed in Figure 6. Both AUCs were statistically significant, demonstrating good overall ability of both methods in distinguishing those patients that were scanned within 4.5 hours from symptom onset. The spherical reference method had a higher AUC (AUC = 0.83, c.i. = 0.70 – 0.96, $p < 0.001$) than the mirror reference (AUC = 0.71, c.i. = 0.55 – 0.88, $p = 0.016$), the former AUC was significantly higher ($p = 0.038$) than the latter.

4. Discussion

We have developed a user-independent method for imaging changes in quantitative cerebral MRI parameters caused by stroke and applied it to determine the change in T2 relaxation time and ADC. We have shown that the method provides data from an animal model for acute stroke that are consistent with the mirror reference method [7] and translated the method to a cohort of human participants. A key development of the spherical reference method here is in generating an image or distribution of the change caused by stroke, accepting that not all voxels are equally affected by ischaemia. The previous mirror-reference approach has sought to deliver a “difference of averages”, with a single measurement value devoid of any measure of uncertainty or heterogeneity (but which is subject to both) [21]. Furthermore, any “difference of average” approach, such as comparison of the mean lesion T2 to mean contralateral T2, ignores the anatomical differences between the voxels sampled in lesion and contralateral reference mask. Our own simulations show that such uncertainty is considerable (data not shown).

We compared the ability of the spherical reference approach with that of the modified mirror-reference method where the non-ischaemic reference is determined by a reflection across the midline. The current way of determining the mirror-reference differs from the originally proposed [21] where the midline is visually inspected and corrected as needed to make selection of homologous region as good as possible whereas in the current approach no user input with midline is needed. Both methods reveal stroke onset time-dependent $\Delta T2$ in the

ADC lesion with comparable ROC characteristics. The spherical reference approach produces less scattered ΔT2 curves and also shows higher sensitivity at maximal specificity than the mirror-reference approach. The latter has an impact when treatment decisions for patients with unknown onset time are to be made to correctly exclude all patients that are beyond 4.5 hours. There are two obvious reasons for improved performance of the spherical reference method. First, the new approach has superior ability to find the reference volume in non-affected brain parenchyma avoiding CSF, thereby making the T2 distribution of the reference volume narrower and, second, the mirror-reference method is prone to misplacement due to inherent asymmetry of brain across the midline. Even a small misplacement will result in inaccurate T2 referencing [18]. Mirror-referencing in ageing brain may be problematic due to volumetric and tissue-related changes, such as white matter T2 hyperintensities.

An angular dependence of T2 has been reported in human WM [11, 14]. The T2 anisotropy has been attributed primarily to result from diffusion-mediated decoherence due to anisotropic susceptibility gradients in WM, and at 3T it leads to variation in T2 up to approximately by 25 ms. The T2 anisotropy is a potential confounding issue for the mirror reference methods, because it uses anatomy as a sole criterion for the contralateral non-ischaemic reference region. The spherical reference method instead should be less vulnerable to such anisotropy because of its voxel-wise intensity-matching algorithm (employing the penalty function).

The time-based restrictions on both rtPA thrombolysis and mechanical thrombectomy mean that if the time of onset cannot be estimated, one or both treatment methods generally become unavailable. This affects a large number of potential recipients of treatment; for example, wake-up stroke occurs in 14 – 24% of cases [19, 22]. These patients are denied treatment, though they may have been within the treatment window. Both CT and MRI have been suggested to estimate whether a stroke has begun within a given time window. Using CT, a correlation between Hounsfield units in the core relative to a contralateral reference has been reported and converted into water uptake [17], reflecting vasogenic oedema. Such a correlation permits estimates of the time of onset, and is reported to have the potential to classify patients with strokes < 4.5 hr with sensitivity and specificity ranging from 79 – 91% and 52 – 85%, respectively. The CT protocol relies on cerebral blood flow data by perfusion CT to delineate the core, however.

MRI using T2-weighted imaging has also been suggested as a method of estimating lesion age with the T2-FLAIR imaging (mainly T2-weighted, but with proton density- and T1-weighted contributions) [25]. This approach exploits a higher signal intensity arising from the lengthened

T2 and increased proton density as the stroke progresses, as proxy of lesion age. However, this signal increase may be counteracted by a T1 contribution, which increases with time after onset in the first hours in animal models [9, 16], decreasing the FLAIR signal. A FLAIR lesion only becomes readily visible to the human eye after some time and the “DWI/FLAIR” mismatch has been suggested as a proxy of lesion age, which assigns a binary value of whether or not a FLAIR and DWI lesion can both be seen [24]. In a trial of 643 patients, it was shown that in the time range 181 – 270 minutes, 53% of patients show mismatch and 47% do not. The technique could classify those <4.5 hr with 62% sensitivity and 78% specificity, and for those <6 hr with 56% sensitivity and 87% specificity. The approach does, however, have the advantage that it suffers little if any confound from other factors [22, 23]. The binary classification using DWI/T2-FLAIR lesion mismatch [24, 28] has proven efficient to triage patients with unknown onset [26].

An image of T2 relaxation time changes has several potential advantages over DWI/T2-FLAIR mismatch, however. First, the competition between contributions to T2-FLAIR intensity, mainly the T1-weighted part [16] which declines over time and therefore opposes the increase in T2 over time, is not present in a quantitative T2 map. Second, an image of T2 change provides the possibility of quantifying how many voxels of the lesion (or beyond) change by a large amount [13, 16]. As such, whilst the average (we suggest median) ΔT2 may be a proxy of lesion age (with error of estimation as not all individuals exhibit the same kinetics), the heterogeneity of ΔT2 may provide some information on how many voxels have transitioned to a T2 reflective of infarction.

A factor that has to be considered when using low-ADC delineation of stroke lesions is that the cerebral blood flow (CBF) thresholds for neurological symptoms and ischaemic energy failure (which triggers the drop in ADC) are different [5]. Animal studies have shown that neurological symptoms appear at CBF levels that are 50 – 60% below the physiological level [5], whereas energy failure and the associated ADC drop have a common flow threshold that is approximately 80% below the normal flow [2]. A further factor to be considered in this disparity is that these CBF thresholds are time-dependent, i.e. in a compromised haemodynamic state, ADC may drop at higher CBF with time than if the occlusion is instantaneous. In animal models the CBF drop to produce energy failure is controlled so that time of ischaemia is explicitly known. Thus, in rat MCAo we have determined the effect of ischaemia on ΔT2, which may not be the case in human patients. In human strokes where

time of ischaemia remains unknown, low ADC will not provide temporal information, rather just presence of ischaemia. In this scenario ∆T2 data from ADC-delineated lesions in rat and human brain may well have different kinetics. In the ischaemic core in rats, T2 initially shortens relative to the non-ischaemic hemisphere lasting for an hour or so before the crossover a to positive gradient appears [3, 7]. The negative ∆T2 results from combined effects of deoxyhaemoglobin build-up and shift of water from the extracellular to intracellular space [13]. In human ADC lesions the ΔT2 versus onset time curves closely resemble those from rats, with a crossover point around 2 hours from onset. A further factor to be considered is that stroke in rat brain is chiefly gray matter, whereas in humans both gray and white matter are affected, and the kinetics of ∆T2 may differ between these tissue types. Despite all the potential confounds, our MRI data indicate that in the ischaemic core ∆T2 increases approximately as much in rats (average 1.9 ms/h) as in humans (average 1.9 ms/h). It should be realised, however, that the percentage change in T2 is greater at 9.4T than at 3T due to shorter parenchymal T2 at ultrahigh field.

4.1. From onset time to tissue characterisation

It is known from animal research that tissue is more probable to become infarcted as its T2 increases [8]. Therefore, an image of the extent to which T2 has increased may eventually be used as a proxy measure of what volume of ischaemic tissue is infarcted and what may still contain salvageable tissue [16]. This is likely to represent a fruitful future use of this methodology. The lesion age is often used as a proxy measure of this, and of the corresponding risk/benefit associated with reperfusion therapy. With additional research, it may be possible to move towards the use of the fraction of lesion tissue with a ΔT2 reflective of infarction and therefore potentially an improved estimate of infarct core.

For now, onset time remains an important parameter for clinical decision making. Our results show that some inference regarding onset time may be made from the median ΔT2 in the ADC-delineated lesion. It is, however, important to recognise that T2 change following onset does not follow ‘one-line-fits-all’ kinetics (evidenced by the animal work), even for voxels in the same lesion within the same individual. As such, the scalar median ΔT2 also has different kinetics for different individuals, and there will be uncertainty in any onset time estimate made based on ΔT2 distributions due to inter-voxel and inter-individual heterogeneity. The uncertainty in onset time deriving from fitting a linear model across the entire cohort of rats was ±2.0 ms (rms), compared to ±5.7 ms in the cross-sectional human cohort. Therefore, ΔT2 provides an onset time estimate but the inherent variation in T2 kinetics across individuals introduces greater uncertainty in humans than in rats.

4.2. Limitations

The current study has some limitations. First, the stroke lesions involved several vascular territories. It is impossible to conclude, from the current data set, whether ∆T2 as a function of onset time is quantitatively uniform in different vascular territories. Second, the majority of patients in the current cohort (66%) were thrombolysed prior to MRI. However, ADC in the stroke lesions was not different between untreated and untreated patients indicating deep ischaemia in both cases. Busch et al. [1] showed in an embolic rat stroke model that in the core with severely lowered ADC rtPA does not influence perfusion, thus in the core rtPA is unlikely to accelerate vasogenic edema. In MCAo rat brain reperfusion leads to recovery of ADC T2, provided ischaemia is short-lasting [10]. We used the same ADC criteria for stroke lesions both in untreated and treated patient, thus in the light of the data above, T2 in the stroke tissue can be assumed to be unaffected by rtPA. Third, the use of T2-weighted signal intensity as reference for choosing voxels in the non-ischaemic hemisphere will inevitably become problematic with time as the time-dependent T2 increase will inevitably also affect T2-weighted signal. Careful inspection of Figure 5c indicates that in the scans acquired with the current parameters, T2 signal intensity shows a positive gradient with time in the ADC lesion beyond several hours. Elevated reference T2-weigthed signal intensity hours after the onset of stroke will diminish ΔT2, thereby underestimating onset time. In such cases, however, visual inspection of T2-weighted and quantitative T2 images may show elevated signal in the ADC lesion. One can reduce the sensitivity of T2-weighted signal to stroke by a suitable choice of TE and TR. Fourth, two types of MRI pulse sequences were used to quantify T2 in humans. These methods yield different absolute T2 from brain parenchyma. As explained in the Method section, the critical parameter used in determining the effects of stroke by both methods is ∆T2, however. In the current data set it is impossible to separate ∆T2s in ADC lesions measured by the two MRI methods.

5. Conclusions

We have shown, using a novel user-independent spherical reference method, that T2 relaxation time increases as a function time from onset in human stroke lesion. The increase is approximately 1.9 ms/h which is comparable to that determined in a rat model of ischaemic stroke. We believe quantitative MRI exploiting T2 and ADC will have clinical impact in stratification of acute ischaemic stroke patients.

Acknowledgements

The study is funded by the Dunhill Medical Trust (grants R385/1114 and OSRP1/1006). Support by the National Institute for Health Research Oxford Biomedical Centre

Programme, the National Institute for Health Research Clinical Research Network, and the Wellcome Trust Institutional Strategic Support Fund (2015-2015) are acknowledged. We acknowledge the support of the National Institute for Health Research Clinical Research Network (NIHR CRN). We wish to acknowledge the facilities provided by Oxford Acute Vascular Imaging Centre.

REFERENCES

1. E. Busch, K. Kruger, P.R. Allegrini, C.M. Kerskens, M.L. Gyngell, M. Hoehn-Berlage, and K.A. Hossmann, Reperfusion after thrombolytic therapy of embolic stroke in the rat: magnetic resonance and biochemical imaging. *J Cereb Blood Flow Metab*. **18**(1998): 407-18.
2. A.L. Busza, K.L. Allen, M.D. King, N. van Bruggen, S.R. Williams, and D.G. Gadian, Diffusion-weighted imaging studies of cerebral ischemia in gerbils. Potential relevance to energy failure. *Stroke*. **23**(1992): 1602-12.
3. F. Calamante, M.F. Lythgoe, G.S. Pell, D.L. Thomas, M.D. King, A.L. Busza, C.H. Sotak, S.R. Williams, R.J. Ordidge, and D.G. Gadian, Early changes in water diffusion, perfusion, T1, and T2 during focal cerebral ischemia in the rat studied at 8.5 T. *Magn Reson Med*. **41**(1999): 479-85.
4. E.R. DeLong, D.M. DeLong, and D.L. Clarke-Pearson, Comparing the areas under two or more correlated receiver operating characteristic curves: a nonparametric approach. *Biometrics*. **44**(1988): 837-45.
5. K.A. Hossmann, Viability thresholds and the penumbra of focal ischemia. *Ann Neurol*. **36**(1994): 557-65.
6. M. Jenkinson and S. Smith, A global optimisation method for robust affine registration of brain images. *Med Image Anal*. **5**(2001): 143-56.
7. K.T. Jokivarsi, Y. Hiltunen, H. Grohn, P. Tuunanen, O.H. Grohn, and R.A. Kauppinen, Estimation of the onset time of cerebral ischemia using T1rho and T2 MRI in rats. *Stroke*. **41**(2010): 2335-40.
8. H. Kato, K. Kogure, H. Ohtomo, M. Izumiyama, M. Tobita, S. Matsui, E. Yamamoto, H. Kohno, Y. Ikebe, and T. Watanabe, Characterization of experimental ischemic brain edema utilizing proton nuclear magnetic resonance imaging. *J Cereb Blood Flow Metab*. **6**(1986): 212-21.
9. R.A. Kauppinen, Multiparametric magnetic resonance imaging of acute experimental brain ischaemia. *Prog NMR Spectr*. **80**(2014): 12-25.
10. M.I. Kettunen, O.H. Grohn, M.J. Silvennoinen, M. Penttonen, and R.A. Kauppinen, Quantitative assessment of the balance between oxygen delivery and consumption in the rat brain after transient ischemia with T2 -BOLD magnetic resonance imaging. *J Cereb Blood Flow Metab*. **22**(2002): 262-70.
11. M.J. Knight, S. Dillon, L. Jarutyte, and R.A. Kauppinen, Magnetic resonance relaxation anisotropy: Physical principles and uses in microstructure imaging. *Biophys J*. **112**(2017): 1517-1528.

12. M.J. Knight, B. McCann, D. Tsivos, S. Dillon, E. Coulthard, and R. Kauppinen, Quantitative T2 mapping of white matter: applications for ageing and cognitive decline. *Phys Med Biology*. **61**(2016): 5587-5605.
13. M.J. Knight, B.L. McGarry, H.J. Rogers, K.T. Jokivarsi, O.H. Grohn, and R.A. Kauppinen, A spatiotemporal theory for MRI T2 relaxation time and apparent diffusion coefficient in the brain during acute ischaemia: Application and validation in a rat acute stroke model. *J Cereb Blood Flow Metab*. **36**(2015): 1232-1243.
14. M.J. Knight, B. Wood, E. Coulthard, and R.A. Kauppinen, Anisotropy of spin-echo T2 relaxation by magnetic resonance imaging in the human brain in vivo. *Biomed Spectr Imag*. **4**(2015): 299-310.
15. E.Z. Longa, P.R. Weinstein, S. Carlson, and R. Cummins, Reversible middle cerebral artery occlusion without craniectomy in rats. *Stroke*. **20**(1989): 84-91.
16. B.L. McGarry, H.J. Rogers, M.J. Knight, K.T. Jokivarsi, A. Sierra, O.H. Grohn, and R.A. Kauppinen, Stroke onset time estimation from multispectral quantitative magnetic resonance imaging in a rat model of focal permanent cerebral ischemia. *Int J Stroke*. **11**(2016): 677-82.
17. J. Minnerup, G. Broocks, J. Kalkoffen, S. Langner, M. Knauth, M.N. Psychogios, H. Wersching, A. Teuber, W. Heindel, B. Eckert, H. Wiendl, P. Schramm, J. Fiehler, and A. Kemmling, Computed tomography–based quantification of lesion water uptake identifies patients within 4.5 hours of stroke onset: A multicenter observational study. *Ann Neurol*. **80**(2016): 924-934.
18. T.J.T. Norton, M. Pereyra, M.J. Knight, B.M. McGarry, K.T. Jokivarsi, O.H.J. Grohn, and R.A. Kauppinen, Stroke onset time determination using MRI relaxation times without non-ischaemic reference in a rat stroke model. *Biomed Spectrosc Imaging*. **6**(2017): 25-35.
19. D.L. Rimmele and G. Thomalla, Wake-Up stroke: clinical characteristics, imaging findings, and treatment option - an update. *Front Neurol*. **5**(2014).
20. J.L. Saver, M. Goyal, A. van der Lugt, B.K. Menon, C.B. Majoie, D.W. Dippel, B.C. Campbell, R.G. Nogueira, A.M. Demchuk, A. Tomasello, P. Cardona, T.G. Devlin, D.F. Frei, R. du Mesnil de Rochemont, O.A. Berkhemer, T.G. Jovin, A.H. Siddiqui, W.H. van Zwam, S.M. Davis, C. Castano, B.L. Sapkota, P.S. Fransen, C. Molina, R.J. van Oostenbrugge, A. Chamorro, H. Lingsma, F.L. Silver, G.A. Donnan, A. Shuaib, S. Brown, B. Stouch, P.J. Mitchell, A. Davalos, Y.B. Roos, M.D. Hill, and H. Collaborators, Time to Treatment With Endovascular Thrombectomy and Outcomes From Ischemic Stroke: A Meta-analysis. *JAMA*. **316**(2016): 1279-88.

21. S. Siemonsen, K. Mouridsen, B. Holst, T. Ries, J. Finsterbusch, G. Thomalla, L. Ostergaard, and J. Fiehler, Quantitative T2 values predict time from symptom onset in acute stroke patients. *Stroke*. **40**(2009): 1612-6.
22. G. Thomalla, F. Boutitie, J.B. Fiebach, C.Z. Simonsen, N. Nighoghossian, S. Pedraza, R. Lemmens, P. Roy, K.W. Muir, M. Ebinger, I. Ford, B. Cheng, I. Galinovic, T.H. Cho, J. Puig, V. Thijs, M. Endres, J. Fiehler, and C. Gerloff, Stroke With Unknown Time of Symptom Onset: Baseline Clinical and Magnetic Resonance Imaging Data of the First Thousand Patients in WAKE-UP (Efficacy and Safety of MRI-Based Thrombolysis in Wake-Up Stroke: A Randomized, Doubleblind, Placebo-Controlled Trial). *Stroke*. **48**(2017): 770-773.
23. G. Thomalla, F. Boutitie, J.B. Fiebach, C.Z. Simonsen, S. Pedraza, R. Lemmens, N. Nighoghossian, P. Roy, K.W. Muir, M. Ebinger, I. Ford, B. Cheng, I. Galinovic, T.H. Cho, J. Puig, V. Thijs, M. Endres, J. Fiehler, and C. Gerloff, Clinical characteristics of unknown symptom onset stroke patients with and without diffusion-weighted imaging and fluid-attenuated inversion recovery mismatch. *Int J Stroke*. **11**(2017): 134-147.
24. G. Thomalla, B. Cheng, M. Ebinger, Q. Hao, T. Tourdias, O. Wu, J.S. Kim, L. Breuer, O.C. Singer, S. Warach, S. Christensen, A. Treszl, N.D. Forkert, I. Galinovic, M. Rosenkranz, T. Engelhorn, M. Köhrmann, M. Endres, D.W. Kang, V. Dousset, A.G. Sorensen, D.S. Liebeskind, J.B. Fiebach, J. Fiehler, and C. Gerloff, DWI-FLAIR mismatch for the identification of patients with acute ischaemic stroke within 4.5 h of symptom onset (PRE-FLAIR): a multicentre observational study. *Lancet Neurol*. **10**(2011): 978-986.
25. G. Thomalla, P. Rossbach, M. Rosenkranz, S. Siemonsen, A. Krützelmann, J. Fiehler, and C. Gerloff, Negative fluid-attenuated inversion recovery imaging identifies acute ischemic stroke at 3 hours or less. *Ann Neurol*. **65**(2009): 724-732.
26. G. Thomalla, C.Z. Simonsen, F. Boutitie, G. Andersen, Y. Berthezene, B. Cheng, B. Cheripelli, T.H. Cho, F. Fazekas, J. Fiehler, I. Ford, I. Galinovic, S. Gellissen, A. Golsari, J. Gregori, M. Gunther, J. Guibernau, K.G. Hausler, M. Hennerici, A. Kemmling, J. Marstrand, B. Modrau, L. Neeb, N. Perez de la Ossa, J. Puig, P. Ringleb, P. Roy, E. Scheel, W. Schonewille, J. Serena, S. Sunaert, K. Villringer, A. Wouters, V. Thijs, M. Ebinger, M. Endres, J.B. Fiebach, R. Lemmens, K.W. Muir, N. Nighoghossian, S. Pedraza, C. Gerloff, and W.-U. Investigators, MRI-guided thrombolysis for stroke with unknown time of onset. *N Engl J Med*. **379**(2018): 611-622.
27. P. Tofts, *Quantitative MRI of the Brain: Measuring Changes Caused by Disease*. 2004, Chichester, England: John Wiley& Sons, Ltd.

28. A. Wouters, P. Dupont, B. Norrving, R. Laage, G. Thomalla, G.W. Albers, V. Thijs, and R. Lemmens, Prediction of stroke onset is improved by relative fluid-attenuated inversion recovery and perfusion imaging compared to the visual diffusion-weighted imaging/fluid-attenuated inversion recovery mismatch. *Stroke*. **47**(2016): 2559-64.
29. Y. Zhang, M. Brady, and S. Smith, Segmentation of brain MR images through a hidden Markov random field model and the expectation-maximization algorithm. *IEEE Trans Med Imaging*. **20**(2001): 45-57.

Table 1. Hyper-acute stroke patient data

Variable	**Hyper-Acute***
Patients	n = 38
Female, n (%)	14 (37%)
Study site, n (%)	
Site 1	19 (50%)
Site 2	15 (39%)
Site 3	4 (11%)
Median age, Y (IQR†)	68 (31 - 85)
Received rtPA before MRI, n (%)	25 (66%)
Median time from rtPA to MRI, hours:mins (IQR)	3:17 (2:09 – 4:30)
Median time from onset to MRI, hours:mins (IQR)	4:21 (1:38 – 9:29)
Median NIHSS‡ on admission, (IQR)	6 (0 - 28)
Stroke subtype§	
Lacunar (LACS)	13 (37%)
Partial Anterior Circulation (PACS)	11 (31%)
Posterior Circulation (POCS)	3 (9%)
Total Anterior Circulation (TACS)	8 (23%)
Left Hemisphere Stroke, n (%)	18 (51%)
Median ADC Lesion Volume, cm^3 (IQR)	1.35 (0.04 - 98.12)

* MRI started within 9 hours of onset; † IQR is interquartile range; ‡ Scores on the National Institutes of Health Stroke Scale (NIHSS) range from 0 to 42, with higher scores indicating greater deficit; § Strokes classified according to the Oxford Stroke Classification Scale.

Table 2. MRI sequence details and acquisition parameters.

Site	T_2 Sequence	T_R [ms]	T_E [ms]	Resolution [mm^3]
Bristol	GRASE	3000	20, 40, 60, 80, 100	0.6×0.6×2.3
Glasgow	TSE	12500	9.5, 66, 123	1.7×1.7×2.0
Oxford	FSE	12000	7.7, 77, 177	1.7×1.7×2.2

Site	T1 Sequence	T_R [ms]	T_E [ms]	Resolution [mm^3]	T_I [ms]	Flip Angle
Bristol	3D FFE	6.84	3.18	1.0×1.0×1.1	N/A	8°
Glasgow	MP-RAGE	2200	2.28	0.9×0.9×0.9	900	9°
Oxford	MP-RAGE	2040	4.55	1.8×1.8×1.0	900	8°

Site	Diffusion Sequence	T_R [ms]	T_E [ms]	Resolution [mm^3]	b-value [s/mm^2] (Multiplicity)	Independent Gradient Directions
Bristol	SE-EPI	3009	60.5	1.2×1.2×4.4	0 (1), 1000 (3)	3
Glasgow	SE-EPI	8000	90	0.9×0.9×2.0	0 (3), 1000 (20)	20
Oxford	SE-EPI	9000	98	1.8×1.8×2.6	0 (1), 1000 (1)	1

LEGENDS TO THE FIGURES

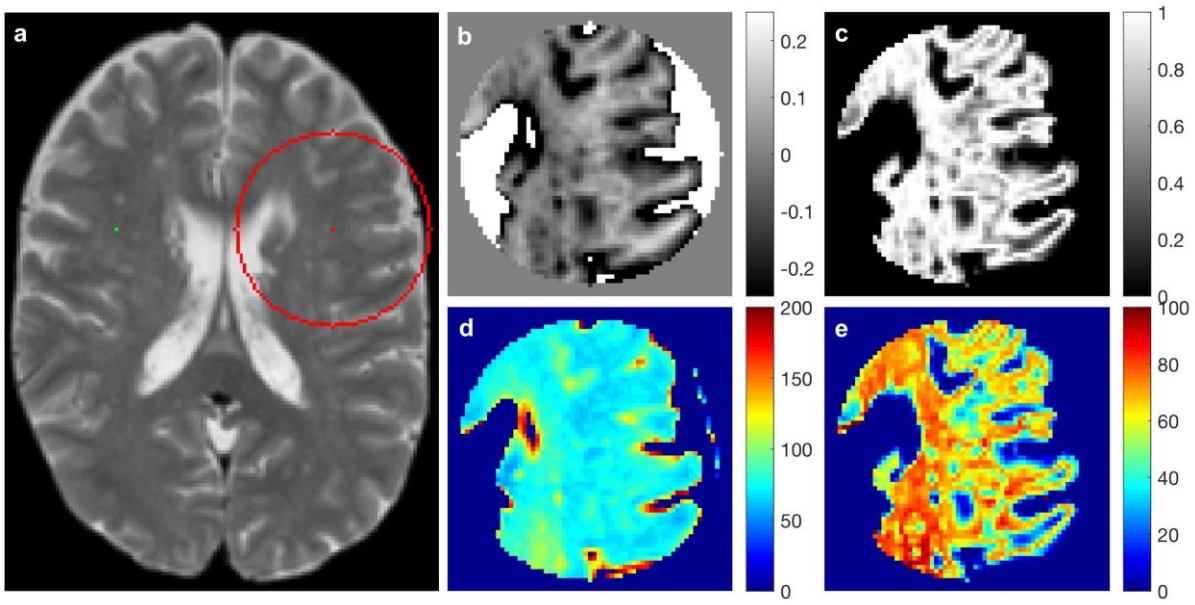

Figure 1: Illustration of the spherical reference method for estimating change due to stroke.

Panel (a) shows a T2-weighted (echo-summed) image from an ADC-negative patient, used here to demonstrate the process applied to ADC-positive patients. The highlighted voxel (green) on the left represents a voxel within a lesion for which an estimate for the pre-ischaemic T2 is required. The red circle (a slice through a sphere) is the reference sphere from which voxels are selected that match the intensity of the 'lesion' voxel. Here, for clarity, the radius of the reference sphere is exaggerated and is usually 2 – 10 mm. Panel (b) shows the normalised intensity difference, $(I^L - I_k)/I^L$, where I^L is the T2-weighted intensity of the lesion voxel (green), and I_k is the intensity of the *k*th voxel within the reference sphere. Panel (c) shows the penalty function with $\sigma = 0.1$, a typical value. Panel (d) shows quantitative T2 values [ms] within the reference sphere. Panel (e) shows a voxel-wise multiplication of the penalty function with the T2 values within the reference sphere. An estimate for the pre-ischaemic T2 is then obtained by summing the voxel values from the images of panels (c) and (e) and normalising the latter by the former.

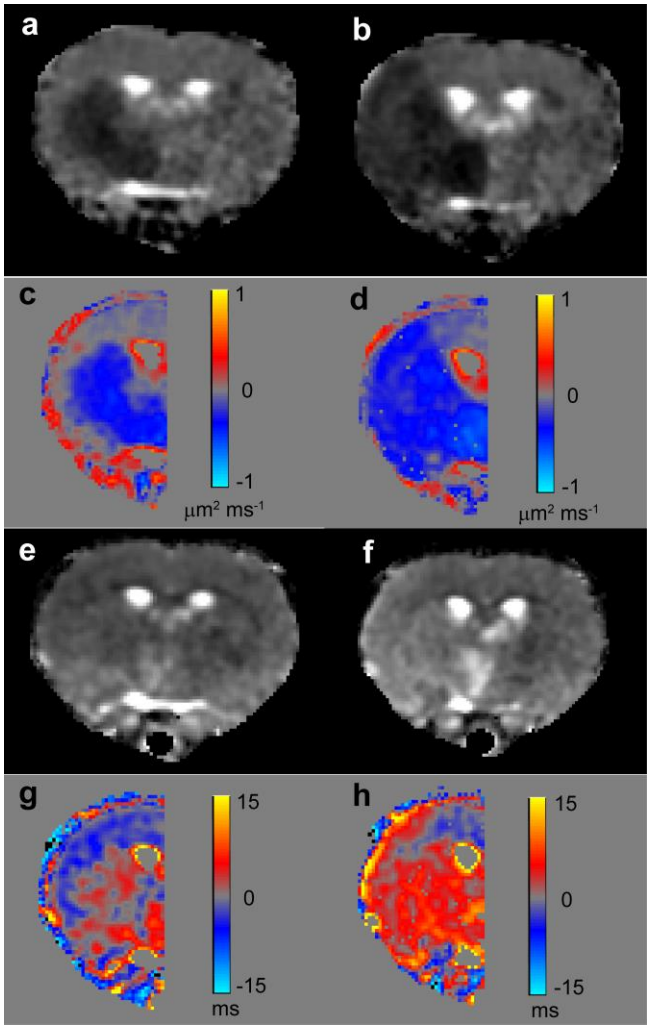

Figure 2: Images of ΔADC and ΔT2 calculated by the voxel-wise parameter change algorithm in a MCAo rat.

ADC (a and b) and T2 (e and f) were acquired at 1 and 4 hours, respectively, from a typical MCAo rat. Panels (c) and (d) are colour-coded ADC images for panels (a) and (b) with values given by vertical reference bars. Panels (g) and (h) are colour-coded T2 images for panels (e) and (f), respectively, with vertical reference bars in ms.

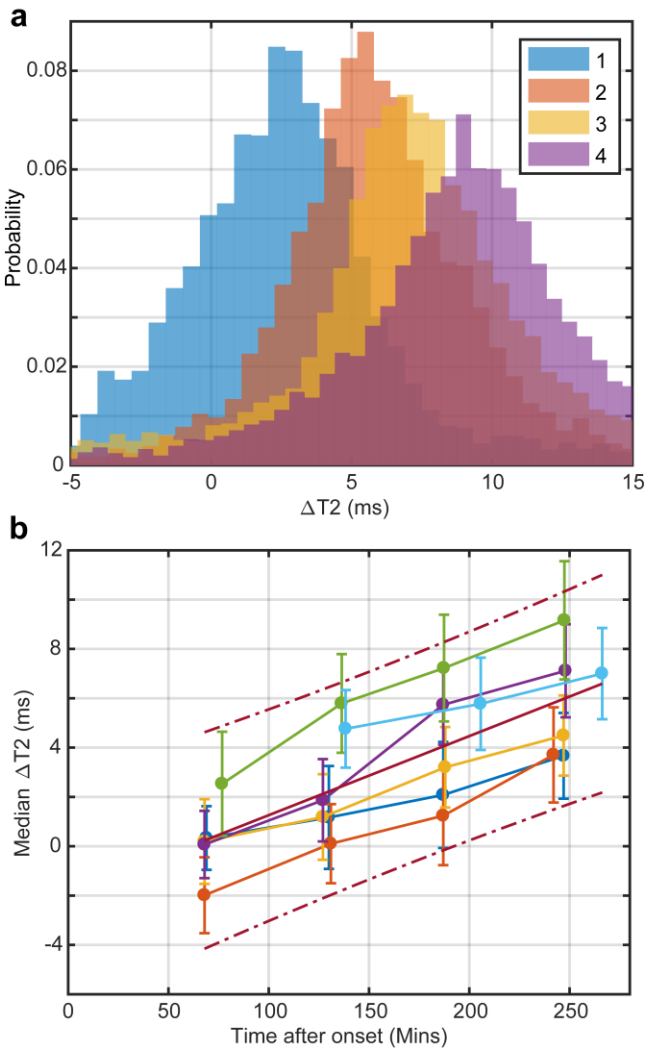

Figure 3: Change of ΔT2 distributions in stroke lesions with time in MCAo rats, calculated using the voxel-wise algorithm.

Panel (a) shows histograms of the lesion ΔT2 distribution at 1, 2, 3, and 4 hours post-occlusion. Panel (b) shows the time course of the median ΔT2 (uncertainties are represented by median absolute deviations of the ΔT2 distribution) in a set of rats.

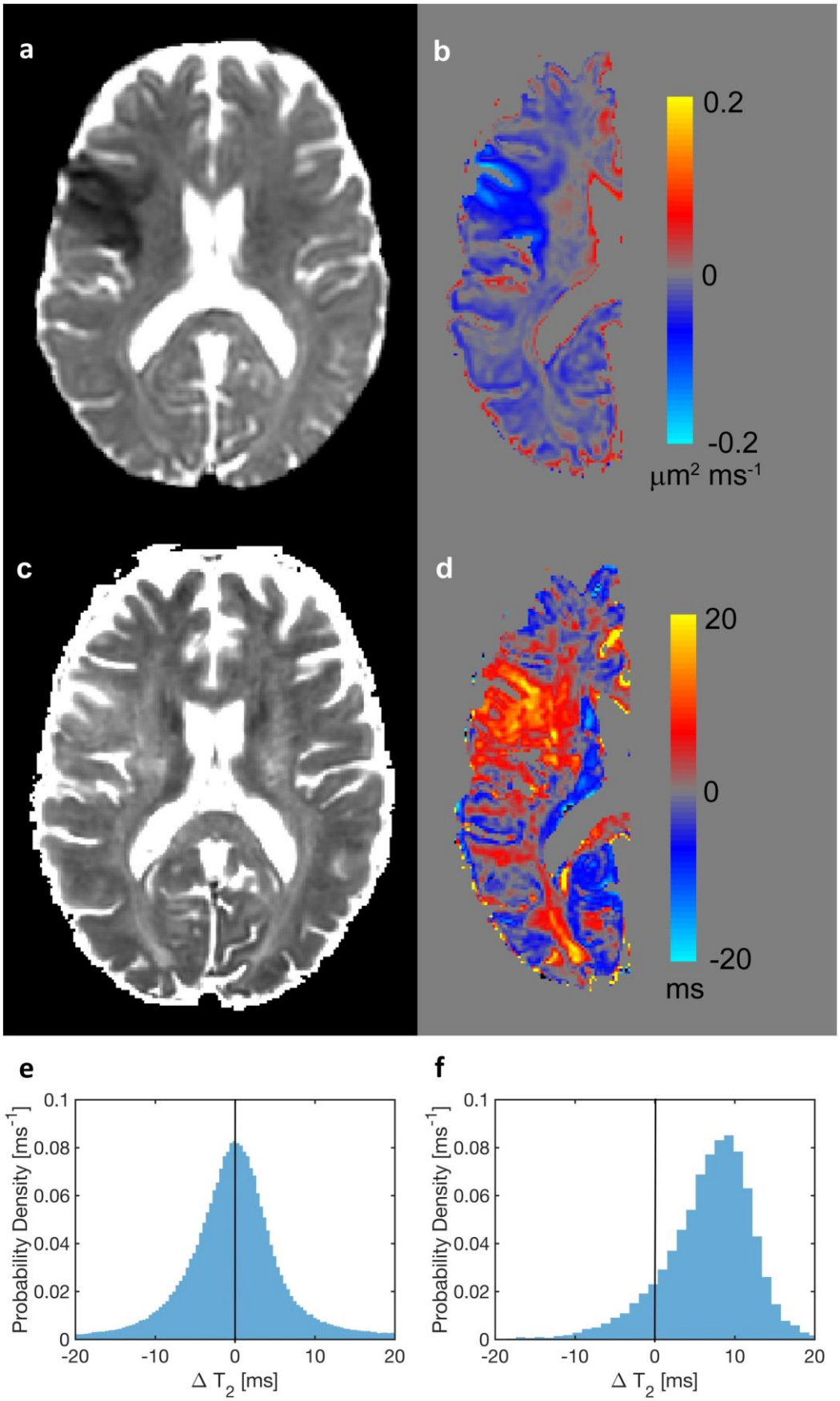
a
b
0.2
0
-0.2
μm² ms⁻¹
c
d
20
0
-20
ms
e
Probability Density [ms⁻¹]
0.1
0.08
0.06
0.04
0.02
0
-20
-10
0
10
20
Δ T₂ [ms]
f
Probability Density [ms⁻¹]
0.1
0.08
0.06
0.04
0.02
0
-20
-10
0
10
20
Δ T₂ [ms]

Figure 4: Estimates of change in quantitative imaging parameters due to acute ischaemic stroke in a patient.

Panel (a) shows an ADC map, with a lesion visible in the right (image left) hemisphere. Panel (b) shows the estimated change in ADC from the pre-ischaemic state. Panel (c) shows a T2 map, panel (d) shows the estimated T2 change from the pre-ischaemic state. Panels (e – f) show ΔT2 distributions: Panel (e) shows the distribution for the normal tissue in hemisphere of the lesion, and panel (f) the distribution in an acute ischaemic stroke lesion.

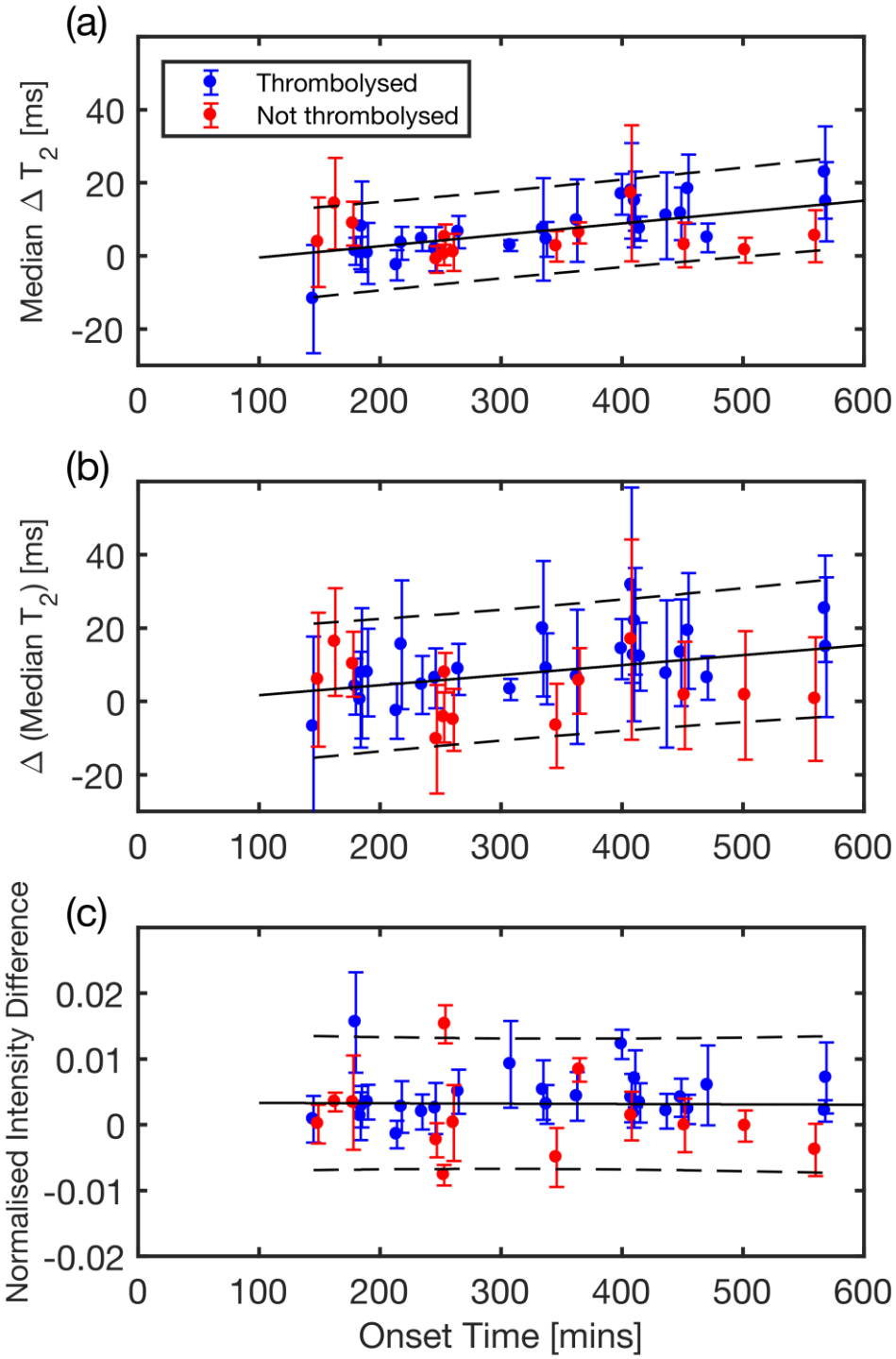

Figure 5: Quantitative relationships between T2 and stroke onset time in human patients.

Panel (a) shows the median ΔT2 (mad with error bars) in the ADC-demarcated lesions against stroke onset time using the spherical reference method. $r^2 = 0.319$, p-value = 0.000222. Panel (b) shows the difference in median T2 between the lesion and its mirrored contralateral region against onset time, $r^2 = 0.139$, p-value = 0.0213. Panel (c) shows T2-weighted signal difference vs time, the slope of the graph is not significantly different to zero.

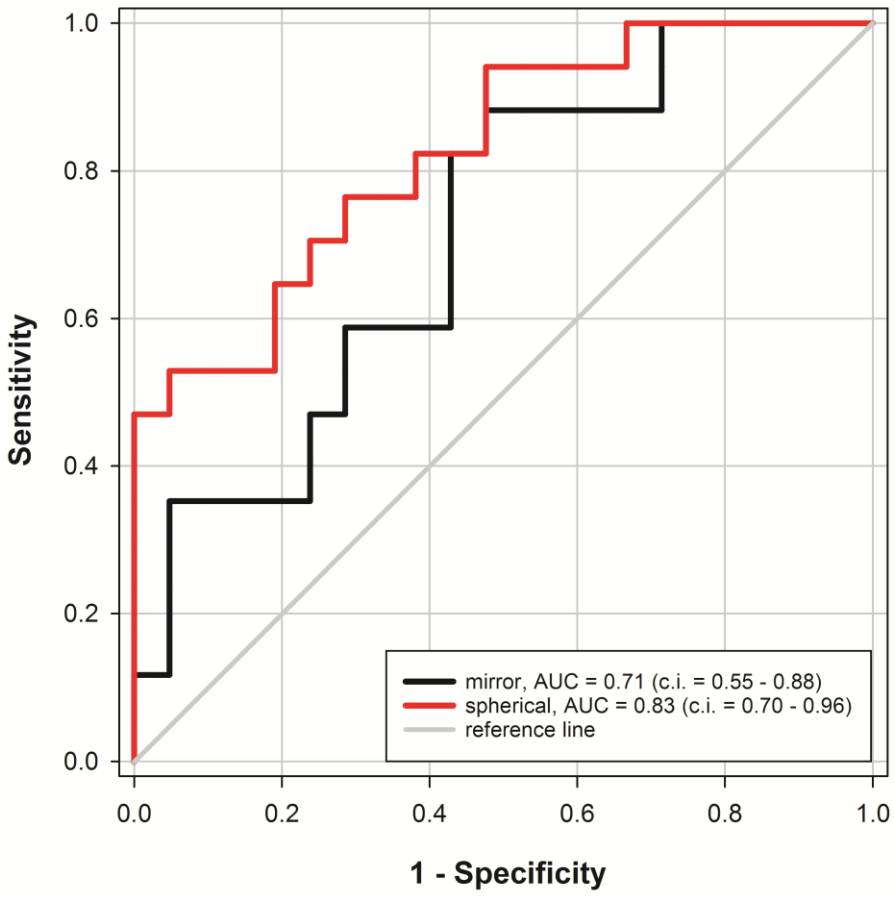

Figure 6: ROCs for the spherical (red line) and mirror reference (black line) approaches for identifying scans performed within 4.5 hours of symptom onset.